



Novel and Green Reduction of Graphene Oxide by Capsicum Annuum: Its Photo Catalytic Activity

Ayesha Hashmi^a, A. K. Singh ^a, Aftab Aslam Parwaz Khan^b, and Abdullah M Asiri^{b,c}

^aDepartment of Chemistry, Government of V. Y. T. PG Autonomous College, Durg, India; ^bChemistry Department, King Abdulaziz University, Jeddah, Saudi Arabia; ^cCenter of Excellence for Advanced Materials Research (CEAMR), King Abdulaziz University, Jeddah, Saudi Arabia

ABSTRACT

Graphene takes concerned noteworthy consideration payable its distinctive thermal, optical as well as mechanical characteristics. There are several chemical methods are available for reduce graphene oxide (r-GO) towards graphene use by many reducing agent's alike hydrazine hydrate and its derivatives. Nevertheless, they are highly explosive and emit harmful gases. Reduction of graphene oxide (GO) employing green approaches by way of plants consumes fascinated much devotion by reason of its competence, sustainable structures, and relatively low in price. Though, the crucial constituents in green extracts and their biological degradation determinations regarding GO continue quiet not well unstated. Now present work, the GO was reduced by *capsicum annuum* (CA) extract. The ideal circumstances for bio reduction existed at volume proportion of chili extract (10 g L^{-1}) and GO (0.5 g L^{-1}) solution aimed at 8 h at 80°C . The r-GO was considered with Raman spectroscopy, Fourier transform infrared spectroscopy (FTIR), Field emission scanning electron microscopy (FESEM), X-Ray diffraction (XRD), Thermo gravimetric analysis/Differential thermal analysis (TGA/DTA), Brunauer-Emmett-Teller (BET), and zeta potential. Outcomes inveterate the oxygen-holding clusters in GO were well detached, development of topping coat on the exterior of r-GO, besides virtuous diffusion of r-GO in aquatic medium. The photo catalytic degradation of GO nano composite was 96% for methyl violet (MV) in 60 minutes.

摘要

石墨烯以其独特的热学、光学和力学特性受到人们的关注。许多还原剂的水合肼及其衍生物可用于将氧化石墨烯 (r-GO) 还原成石墨烯用途。然而，它们具有很强的爆炸性，并释放有害气体。氧化石墨烯 (GO) 以其具有竞争力、结构可持续性和价格相对低廉等优点而备受关注。然而，绿色提取物中的关键成分及其对GO的生物降解测定尚不清楚。目前的工作是用辣椒提取物降低GO。生物还原的理想条件为辣椒提取物 (10 g L^{-1}) 和GO (0.5 g L^{-1}) 溶液在 80°C 下8h的体积比。利用拉曼光谱、傅立叶变换红外光谱 (FTIR)、场发射扫描电子显微镜 (FESEM)、X射线衍射 (XRD)、热重分析/差热分析 (TGA/DTA)、布鲁纳-埃米特-特勒 (BET) 和zeta电位对r-GO进行了研究。结果表明，GO中的含氧团簇分离良好，除在水介质中有良好的扩散外，表面有涂层的发育。GO纳米复合材料对甲基紫 (MV) 的光催化降解率为96%。

KEYWORDS

GO; capsicum annuum; green reduction; photocatalytic activity

关键词

辣椒; 绿色减排; 光催化活性

CONTACT A. K. Singh  ajayksingh_au@yahoo.co.in  Department of Chemistry, Government of V. Y. T. PG Autonomous College, Durg 491001, India; Aftab Aslam Parwaz Khan  draapk@gmail.com  Chemistry Department, King Abdulaziz University, Jeddah 21589, Saudi Arabia

 Supplemental data for this article can be accessed [here](#).

© 2020 Taylor & Francis

Introduction

Graphene is a regular mono-layer carbon atom with hybridized of sp^2 and compactly organized with honeycomb like structure. Conductivities abilities to have a molecular barrier (Cui, Kundalwal, and Kumar 2016) and superior mechanical properties are some significant properties that causes graphene to be have uncountable exploration effort to integrate graphene in polymeric design of nanocomposites (Xiao et al. 2002; Li et al. 2011). Van der wall interaction troubles the usage of pristine graphene leading to difficulty in bottom-up approach of synthesis cause by less solubility (Niyogi et al. 2006) there by leads to agglomeration in-situ. With top-down process for the merits of pristine graphene by saturating its surface by the functional oxygen group. The formation of graphene oxide (GO) by oxidation of carbon graphite or different carbon allotropes (fullerene, carbon nanotube, etc.). The oxidation of graphite in protic solvent leads to graphite oxide with multiple layers of stacked GO over one and another.

GO has a comparable hexagonal closed packing (hcp) like carbon structure to graphene with the basic functional assemblies like alkoxy (C–O–C), carboxylic acid (–COOH), carbonyl (C–O), hydroxyl (–OH), and other oxygen based on functional assemblies (Pendolino and Armata 2017). For synthesis of GO there are several method are accessible like chemical vapor deposition (CVD) (Niasari, Ghanbari, and Estarki 2012), microwave-assisted method (Mohandes, Davar, and Niasari 2010) chemical approaches (Xie, Forslund, and Pan 2014), etc. Amongst these techniques, the chemical way constructed on the reduction of GO in large-scale production. Hydrazine hydrate and its derivatives are extensively show a vital part in the reduction of GO. Inappropriately, highly toxic and hazardously unstable it is holder with excessive carefulness. Yet, because of its toxic behavior alternative green reductant is intensely recommended. In modern phase, there are many green way by naturally occurring reducing agents were used for reduction of GO (Akhavan and Ghaderi 2012), and (Guo et al. 2009). Furthermore, GO and r-GO have wonderful prospective for many biomedical utilizations like drug delivery, tissue engineering, bioimaging, tissues stitching by resident warming, purify biological fluids, battered drugs or genes transport, divergence negotiators in MRI, etc. (Gong et al. 2009; Zhang et al. 2014) owing to their good bio-stability. Thus, here is an emergent necessity to progress ecologically responsive production procedures for these graphene's that whichever does not practise lethal chemicals. Enlargement of L-cysteine and an amino acid to produce r-GO and discovered its photo catalytic action on methylene blue (MB) (Yusuf et al. 2015).

For the preparation of graphene, flower petals (Ray et al. 2012) are used as a carbonaceous source and wild carrot (Kuila et al. 2012) as a mild reducing agent.

At present, we made-up GO over a modified Hummers method and shortened it in r-GO by using the organic and natural reluctant (Niyogi et al. 2006). Green chili (*Capsicum annum*) have been a common spice and traditional medicine in several region of world. It has contained hydroxyl cluster (–OH) in the aromatic ring and contain amide moiety. Position of hydroxyl cluster and its length decides the amount of spiciness of chili berries (Jha and Prasad 2011). A wide spectrum of antioxidants compounds is present in chili fruits, which prevent proliferation of oxidative chain. All chili papers, including green chilies, encompass capsaicin (8-methyl-*N*-vanillyl-6-nonenamide) which is liable for the spicy sensation associated with eating a hot pepper. Phenolic compound present in chili fruit has great tendency to retard the lipid autoxidation by acting as radical scavengers (Namiki 1990). One of the major carotenoid presents in chili, β -carotene which act together with free radicals and act like a chain breaking antioxidants (Palozza and Krinsky 1992). One of the most powerful natural antioxidants is lycopene by way of a contributing factor in reducing the impermanence from numerous cancer cells (Gerster 1997). Numerous dye industries are comprising polluting water bodies and causes serious environmental and health problems (Motahari et al. 2013). Decomposition of these polluted fragments since water is an immense anxiety (Davar et al. 2010).

Carbon-based and other 2D materials have been employed in the adsorption process toward removal of organic and inorganic impurities (Zhang et al. 2014). Nowadays, r-GO has highly applicable for various dye adsorption (Mahmoodi et al. 2017), r-GO considered for the adsorptive removal

of dye because due to presence of oxygen functionalities, laterally with some fault in graphitic spheres (Minitha et al. 2017). Mostly, r-GO intermingle with dyes over hydrophobic connotation, *p-p* interaction, electrostatic interaction, etc. these types of contacts capable for the adsorption of dye on r-GO surface (Zhu et al. 2013). Dye adsorption capacity has improved by the large surface area of r-GO with high porosity, and this is possible by controlling the quality of the precursor used for GO and selected reduction methods used. Presently, GO and r-GO-based nanocomposites are used as a photocatalyst for the degradation of dyes in wastewater management (Liu et al. 2017; Pavoski et al. 2017; Noha et al. 2019). Nowadays, photocatalytic degradation has been used as an implement for demonstrating the technical welfares of photocatalysis. Usually, electron is excited when the band gap of the photocatalyst is equal to or lower than the energy of light absorbed and thereby developing electron and holes. For production of reactive oxygen species (ROS), photogenerated electron-hole pairs utilizes the surrounding water molecules and oxygen, which are ultimately accountable to break down of dye molecule (Alsebaei et al. 2018). There were many studies which shows the use of r-GO by means of photocatalyst in the elimination of dye pollutants, especially extraction of harmful methylene blue from wastewater. There is lack of knowledge about the optimization of its photo-activity, despite that it also shows excellent ability to absorb MB. Other than that, r-GO act as semiconductor, it is environment friendly material, plus it is inexpensive, r-GO shows great potential to be used as metal free photocatalyst, which also aid the nature through its environment friendly properties.

In this paper, the conversion of GO to r-GO was considered by several performances like XRD, FTIR, TGA/DTA, FE-SEM, Raman, zeta potential, and BET measurement. Suggested synthesis appliance to reduce GO over CA is eco-friendly and cost effective too. The competence of as organized r-GO in dye adsorption was also examined. Dye elimination determination of MV, which is comprehensively likely in dye industry to dye clothes, paper, leather, etc. remained executed by r-GO.

Results and discussion

XRD is mainly advantageous for the determination of lattice parameter of the crystal organization. Figure 1 displays XRD outlines of CA extract, GO, and r-GO. The XRD outline of CA extract shown in Figure 2, for CA peak at $2\theta = 21.6^\circ$ (Alsebaei et al. 2018) and 23.9° (d-spacing = 0.3915 nm) and GO

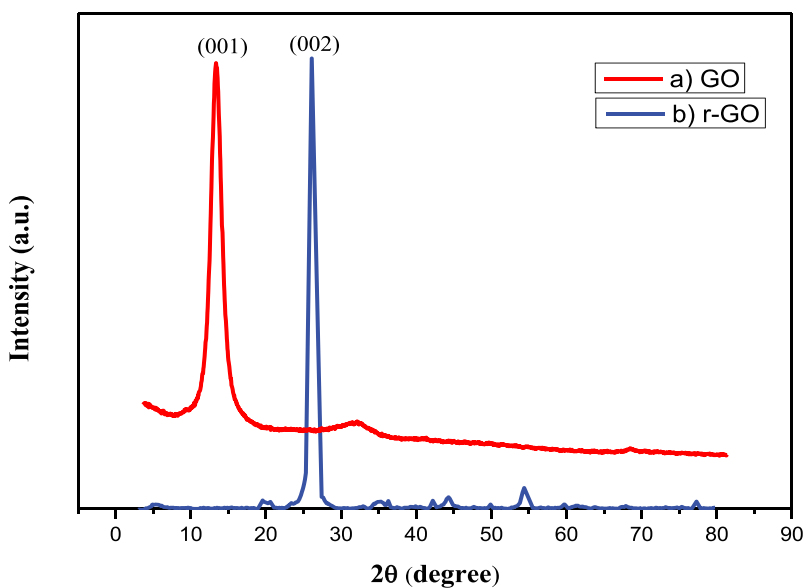


Figure 1. XRD images of (a) GO and (b) r-GO.

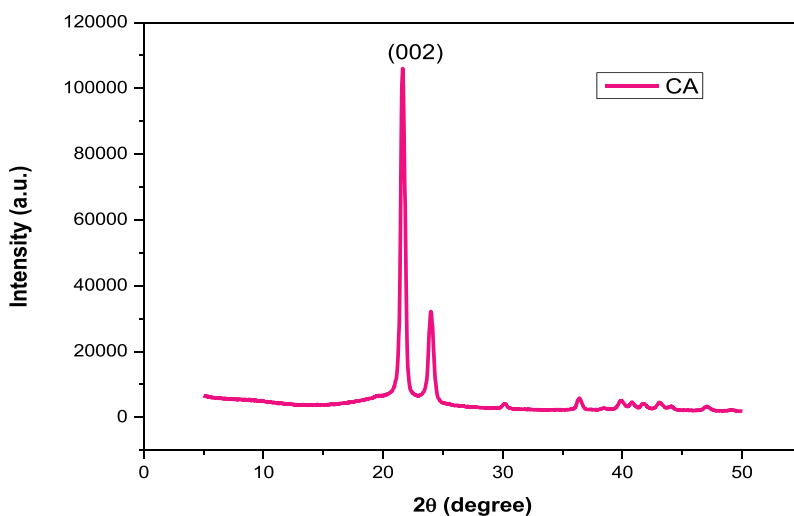


Figure 2. XRD images of CA.

shows a sharp tip on $2\theta = 10.6^\circ$ (d-spacing = 0.8352 nm) conforming toward 001 likeness about the graphitic construction. The d-spacing increases because of the introducing containing water residues along with the construction of oxygen affiliation in the intermediate layer arrangement of graphite. After reduction of GO to r-GO, the 002 consideration peak at lower angle disappeared and an extensive peak at about $2\theta = 26.1^\circ$ (d-spacing = 0.3414 nm) was observed. It indicates that the excessive reduction and exfoliation of GO and fabrication of r-GO. The comprehensive conversion from GO to r-GO is evidently demonstrated separately vanishing of the 002 reflection route by not at all different deflection peaks in the XRD arrangement is found. Table S1 Demonstrate the grain size, d-spacing, reflections of obtained GO and r-GO. The XRD arrangement of r-GO is such of a crystalline solid (Hashmi et al. 2020a). Here Table 1 Evaluate the interlayer spacing of GO and r-GO by using various reductant. Average crystalline size of particle was calculated by Scherrer's equations as follows (Hashmi et al., 2020b).

$$D = K\lambda/\beta\cos\theta$$

Where, D = crystalline size of the particle, K is a constant (0.89), λ the X-ray wavelength (0.1541 nm), β the full width at half maximum in radian (FWHM), and θ is the diffraction angle.

d- Spacing is determine by using Bragg's equation.

$$2d \sin\theta = n\lambda(2)$$

Where d is the interplanar distance between lattice planes and n is an integer.

Figure 3 displays the FTIR bands recorded for CA extract and GO before then after reduction. The FTIR bands of CA extract shows peak on 3311 cm^{-1} due to hydroxyl stretching, 1597 cm^{-1} is due to restoration of aromatic ring and peak at 1013 cm^{-1} is due to epoxy group. GO displays peak on 3235 cm^{-1} due to hydroxyl cluster, peak on 1591 cm^{-1} attributed due to the restoration of aromatic

Table 1. Evaluation of interlayer spacing of GO and r-GO by using various reductant.

Reducing agents	$2\theta(\text{GO})$	d- spacing (GO) in nm	2θ (r-GO)	d-spacing nm	Ref.
Phytoextract	9.75°	0.906	25°	0.360	Thakur and Karak (2012)
Carrot root extract	11.2°	0.79	23.96°	-	Kuila et al. (2012)
Tannin	9.7°	0.90	26.3°	0.340	Lei et al. (2011)
Tea extract	9.6°	0.92	24.6°	0.340	Wang, Shi, and Yin (2011)
Caffeic acid	10.02°	0.880	24.79°	0.359	Bo et al. (2014)
Capsicum annum	10.6°	0.8352	26.1°	0.3414	This work

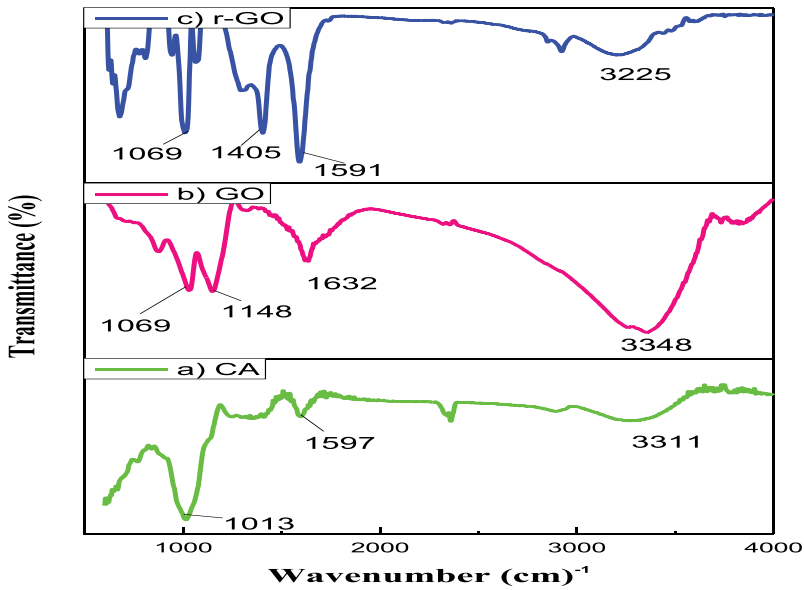


Figure 3. FTIR spectra of (a) CA, (b) GO, and (c) r-GO.

ring. Peak on 1405 cm^{-1} is because of $\text{C} = \text{C}$ extending frequency. The intensities of peaks conforming toward oxygen functionalities namely the $\text{C} = \text{O}$ extending vibration peak then the $-\text{OH}$ distortion peak falls prominently later 12 h, representative that GO remained diminished. Figure 3 furthermore displays a reduction of GO. Peak on 3348 cm^{-1} is recognized due to hydroxyl functional cluster in alcohol and phenolic compound. The groups at 1632 cm^{-1} is because of $\text{C} = \text{C}$ extending frequency and peak at 1169 cm^{-1} due to $\text{C}-\text{O}$ extending mode. Here Table 2 demonstrate FTIR studies of GO using different reducing agents.

From FTIR peak area analysis of hydroxyl cluster for CA extract, GO and r-GO (Figure 3 and Table 3), the decrease in the peak extent was detected. It may be considered that the curve was nearly flattened for sample r-GO. The peak at 3448 cm^{-1} as assigned to OH stretching vibration mode was therefore started to decrease.

Figure 4 and 5 illustrate the TGA/DTA of GO and r-GO were examined under N_2 atmosphere. GO displays a weight loss around 4.72% below 100°C as a consequence of the discharge of absorbed water, and an additional rapid weight loss about 11.96% from 100 to 250°C which is recognized to the

Table 2. FTIR studies of GO using different reducing agents.

Reducing agents	-OH	C-O	C-O	C-OH	OH-	Ref.
Lemon wine	3450	N/A	1409	1660, 1600	N/A	Gurbani et al. (2018)
Reusable K_2CO_3	N/A	1227	1409	1733	1404	He et al. (2015)
Rose water	3408	1048	1359	1719	N/A	Haghighi and Tabrizi (2013)
Reducing sugar	3403	N/M	1600	N/A	1395	Zhu et al. (2010)
Super critical alcohol	3380	1220	1050	N/A	N/A	Seo et al. (2013)
Capsicum annum extract	3348	1148	1069	N/A	N/A	This work

Table 3. Peak area analysis of hydroxyl group for GO and r-GO.

Samples	Area GO	$A_{r\text{-GO}}$	$A_{r\text{-GO}} - A_{\text{GO}}$	$\left(\frac{A_{\text{GO}} - A_{r\text{-GO}}}{A_{\text{GO}}}\right) \times 100$	Reduction %	References
$A_{r\text{GO}}$	188.35	529.44	341.09	0.644	64.42	Dutta, Thiyagarajan, and Bahadur 2016
rGO-3	145.54	529.44	383.9	0.725	72.51	
rGO-7.5	390.94	529.44	138.5	0.261	26.16	
rGO-12						
C-GO	345	49	296	0.857	85.7	This work

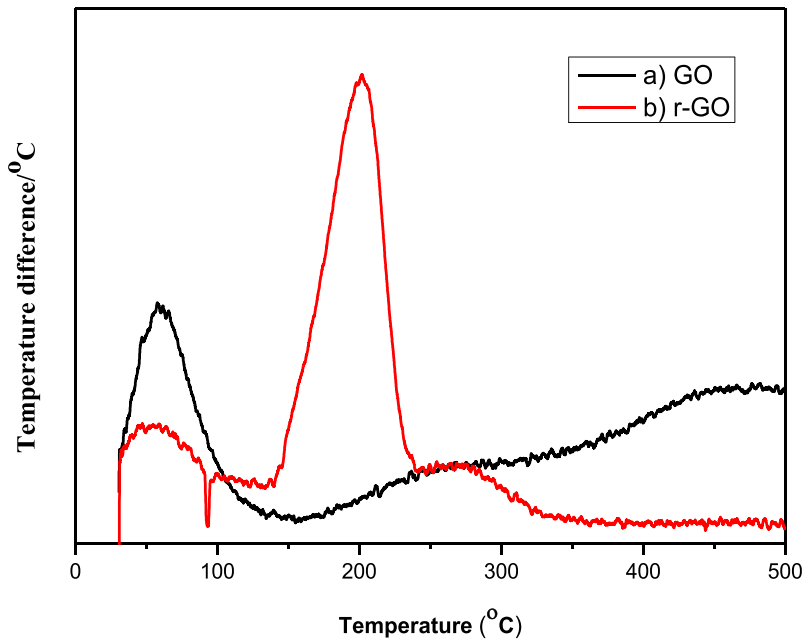


Figure 4. DTA images of (a) GO and (b) r-GO.

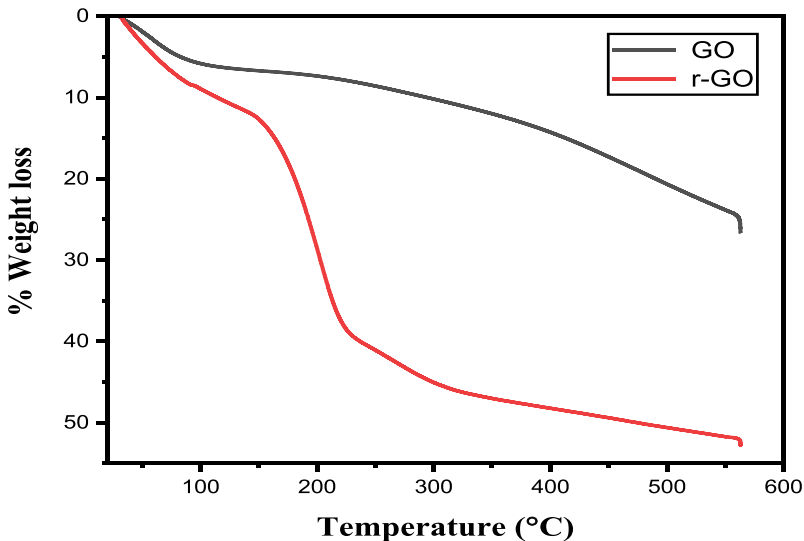


Figure 5. TGA plots of (a) GO and (b) r-GO.

deduction of the oxygen enclosing functional assemblies that produce CO, CO₂, and water. The weight loss of GO at 800°C is about 16.68%. After reduction, the r-GO attribute total weight loss around 12.01%. This result shows CA is superlative for the reduction of GO and diminishing the aggregate of oxygen comprising functional clusters (Pimenta et al. 2007). Figure 5 shows DTA curve for GO and r-GO shows exothermic reaction.

Field emission- scanning electron microscopy is generally used to determine the morphology of the substances with higher resolution. Generally, GO appears as wavy wrinkled structures with blurry

edges (He and Gao 2010). When increasing the concentration, GO surface looks like flooring appearance which is due to be the addition of remaining water moieties, carboxyl, and hydroxyl groups. In case of r-GO it looks like thin and wrinkled structure which is due to the assembling of discrete sheets by flat pack practices (Toh et al. 2014). The surface morphologies by FE-SEM determination of the prepared GO and r-GO are revealed in Figure 6(a and b). The typical uneven and crumpled graphene sheets assembled of lots of fixed layers with frequent boundaries are detected in Figure 6(a). The flake-like sheets of the arranged r-GO are visibly detected in Figure 6(b).

Raman spectroscopy is generally useful for the determination mechanical and electrical properties of graphene with structural deficiency, imperfection density and fixing level of GO and r-GO. In the Raman spectrum (Figure 7) of greatly ordered graphite a pair of absorption band, so entitled G and D bands, are recognized as frequencies less than 2000 cm^{-1} . The G band is frequently dispersed to the E_{2g} phonon of sp^2 carbon atoms, the in-phase vibration of graphite framework, and it seems at almost 1575 cm^{-1} and characterize the comparative degree of graphitization. D band is a fragile conscious mode of K-point phonons of A_{1g} symmetry and it is produced by the graphite edges. It seems at almost 1355 cm^{-1} and its intensity is correlated to the degree of edge chirality. The ratio of D and G band intensities (ID/IG) designates the degree of the complaint such as imperfections, wrinkles, and edges. In the Raman spectrum of exfoliated GO as the amorphous carbon encompasses a convinced fraction of sp^3 carbons, the G band is expanded and transfers upwards to upper frequencies and the intensity of the D band rises extensively. So, the broad oxidation organized with ultrasonic exfoliation declines the extent of in-plane sp^2 territories and enriches the disorder i.e. ID/IG fraction. The Raman spectrum of the prepared exfoliated GO exhibited two absorption peaks at about 1298 cm^{-1} and 1587 cm^{-1} for D and G bands individually, while the prepared r-GO established D and G bands at 1288 cm^{-1} and 1584 cm^{-1} , individually (Figure 7). The 2D signal of the organized r-GO was at about 1738 cm^{-1} .

ID/IG ratio for r-GO was about 1.30 and advanced than that experiential for the exfoliated GO i.e. 0.83. The decline of the ID/IG ratio is expected for r-GO subsequently reduction of exfoliated GO because of the reestablishment of the sp^2 domain. It appears the obtained r-GO are break down into lesser fragments in the progression of the chemical reduction of exfoliated GO and afterward the size of the sp^2 domains falls. An analogous surveillance in which the ID/IG ratio is improved subsequently

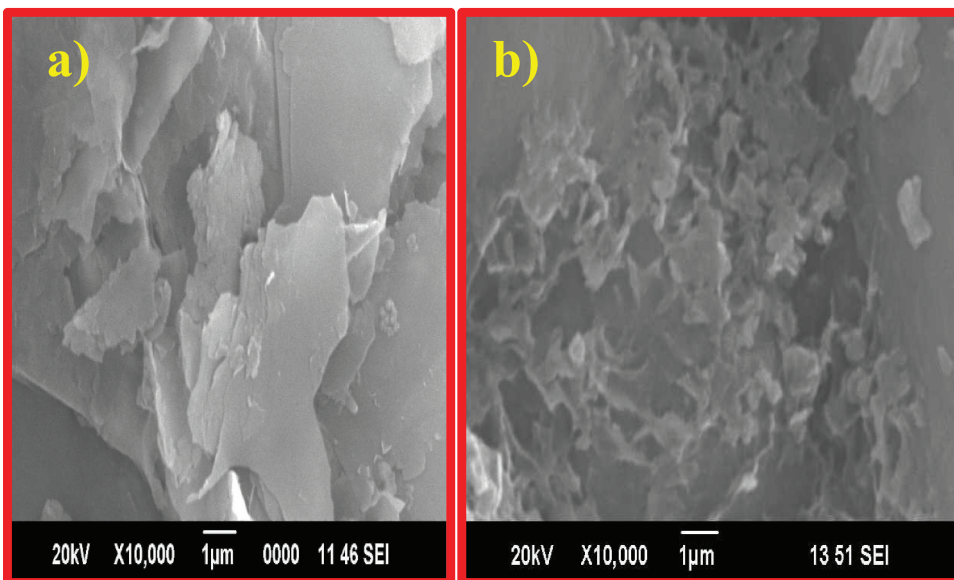


Figure 6. FE-SEM images of as synthesized (a) GO and (b) r-GO.

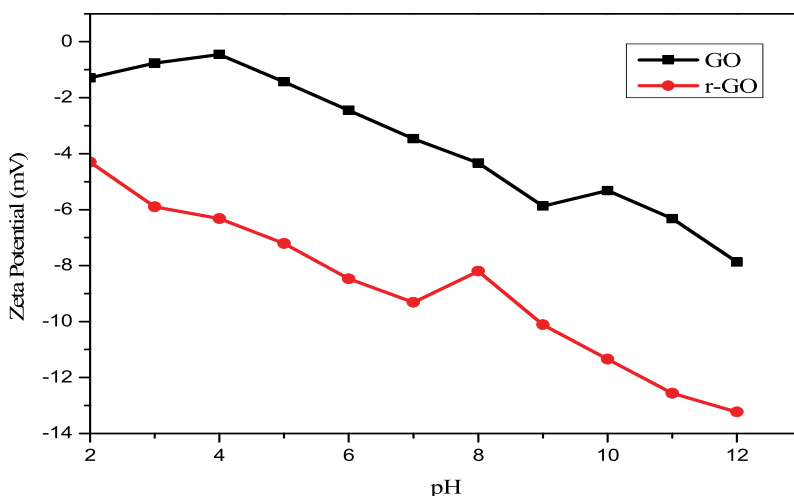


Figure 7. Zeta potential of GO and r-GO.

Table 4. Comparison of ID/IG ratio of GO and r-GO using different reducing agents.

Reducing agents	ID/IG ratio for GO	ID/IG ratio for r-GO	Ref.
Vitamin C + amino acid	1.56	1.75	Gao et al. (2010)
Vitamin C/L-ascorbic acid	0.95	1.2	Fernandez-Merino et al. (2010)
Natural cellulose	1.32	1.53	Peng et al. (2012)
E. coli	1.37*	0.97*	Akhavan and Ghaderi (2012)
Capsicum annum extract	0.83	1.30	This work

the chemical reduction of GO has been reported (Shulga et al. 2014). Here Table 4 shows comparison of ID/IG ratio of GO and r-GO using different reducing agents.

Figure 8 characterizes the zeta-potential of the GO and r-GO against pH. In general study, when the value of zeta potential is high for colloidal particle, then they transverse to one another and diminish affinity to flocculate. On the other hand, when the colloidal particle have low zeta potential value than small repulsive force work on them, foremost to agglomeration (McAllister et al. 2017). Zeta potential of colloidal particle is generally affected by the pH value of collides. When the value of zeta potential is further positive than +30 mV or further negative than 30 mV, collide deliberated to be unchanging. Figure 8 demonstrates, all the GO, r-GO suspensions would become stable once the zeta potential ranges come to be ≤ -30 mV in the pH range of 9–12. Importantly, the r-GO must stay familiar on in elevation negative zeta potentials via cumulative pH, which approves a shallow inclination of r-GO sheets underneath the applied voltage. On 10 pH the value of zeta potential for GO and r-GO is -5.35 mV and -11.33 mV respectively.

BET surface area determination

Nitrogen adsorption–desorption isotherms as well as pore size distribution of GO and r-GO are demonstrated in Figure S1 at 77 K. It can be determined that synthesis of GO through the chemical method is considered by the expressively a lesser amount of developed specific surface area ($3 \text{ m}^2 \text{ g}^{-1}$). This divergence may be elucidated through the point that a growth in BET surface area is correlated by the deteriorating of graphene film organization. Therefore, it may be specified that graphitic arrangement of GO fabricated via chemical way is conserved in upper step as paralleled to GO synthesized by Hummers scheme. By cause of reduction of GO (Figure S2), surface area amplified basically after 3 for GO just before $40 \text{ m}^2 \text{ g}^{-1}$ for r-GO. Overall pore volume upsurges extremely after reduction–

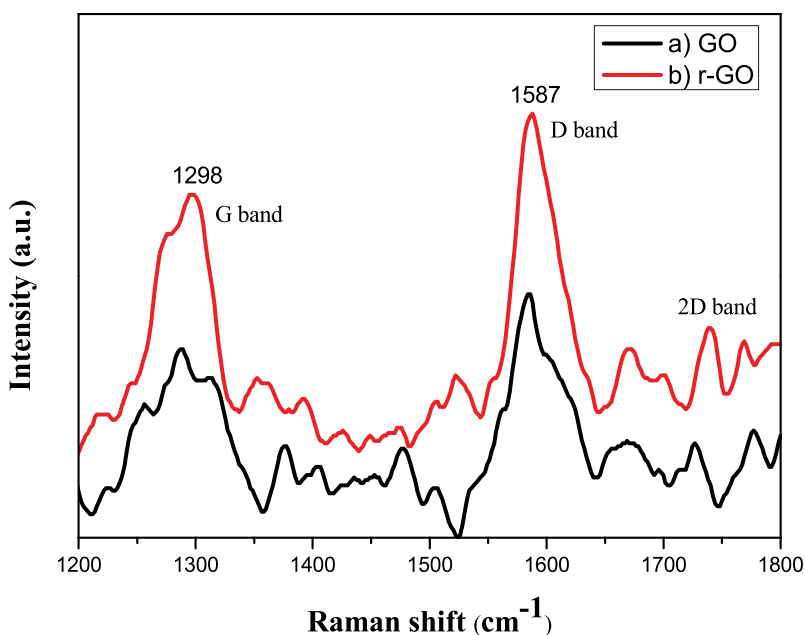


Figure 8. Raman spectra of (a) GO and (b) r-GO.

exfoliation progression since $0.03\text{--}1.5\text{ cm}^3\text{ g}^{-1}$ for GO and r-GO, individually (Figs S3 and S4). These outcomes justify the report that the pore organization of r-GO from electrochemically acquired GO is much nearer to that distinguished for the r-GO prepared on the root of Hummers scheme. Since the works it is recognized that dependent on flake circumstances corresponding temperature, atmosphere, time period, the specific surface area of r-GO series from $300\text{ to }800\text{ m}^2\text{ g}^{-1}$ whereas typical pore extent after $2\text{ to }20\text{ nm}$ (Chen et al. 2012).

UV-Visible spectroscopy

Here, UV-Vis absorption spectra recorded for GO and r-GO, shown in (Figure 9). An absorption peak for GO was found at 229 nm due to $\pi\text{-}\pi^*$ transition of the aromatic C-C bond and for r-GO absorption peak was red-shifted obtained around 262 nm due to the $n\text{-}\pi^*$ transition of C = O bonds. In this condition change in color found to be light brown to black due to the incomplete restoration electronic conjugation, p network, inside the graphene sheets under reduction of GO.12,27 (Zhu et al. 2010;).

Dye removal study

Adsorption study of methyl violet (MV)

MV is a cationic colorant, IUPAC term Tris (4-dimethylamino)phenyl)methylm chloride. Molecular formulation $\text{C}_{25}\text{N}_3\text{H}_{30}\text{Cl}$ and molecular weight 393.959 g/mol . During spectrophotometric evaluation it display maximum spectra at 584 nm . In current study, MV was purchased from Merck and its 100 ppm standard solution was primed in double de-ionized water. The preferred concentrations of MV was carried out by gradual dilution process aimed at the stock solution. Toward study the dye elimination competency of r-GO, MV dye was castoff. About 10 mg r-GO was put in 100 mL MV solution (5 ppm). The mixture was continuously stirred on orbital shaker at 25°C by 150 rpm . Figure

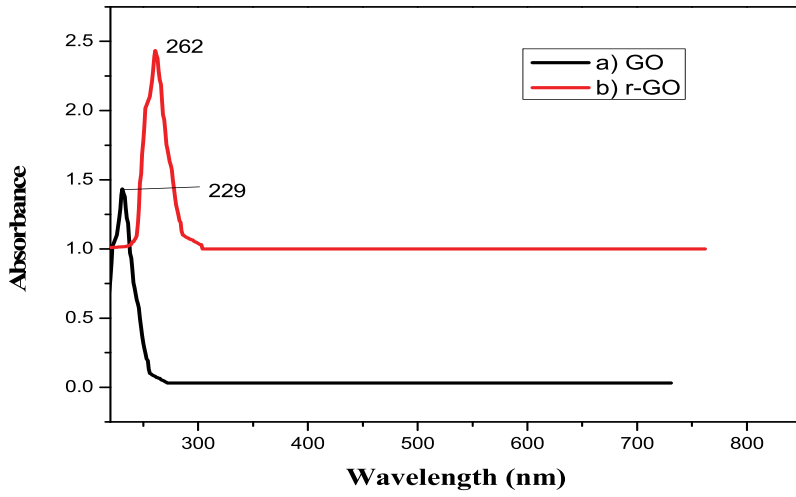


Figure 9. UV-Visible spectra of (a) GO and (b) r-GO.

10 shows a removal of MV dye using r-GO at 60 min. A fixed volume of the dye solution was taken out after regular time intervals and centrifuged for the removal of r-GO.

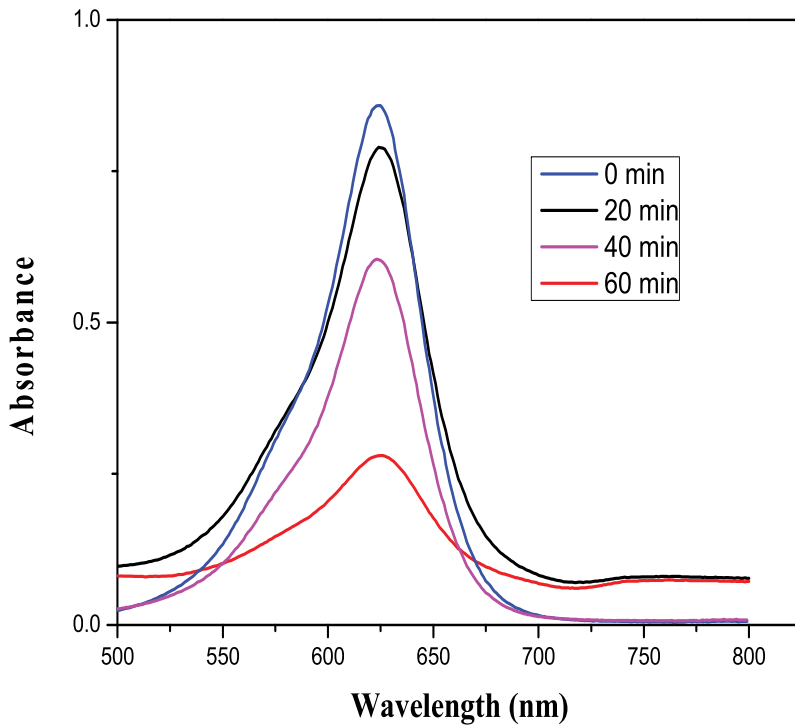


Figure 10. Removal of MV dye using r-GO.

Mechanism behind the heterogeneous photocatalytic degradation

Heterogeneous photocatalytic degradation is a cost-effective technique for wastewater treatment which speed up photoreaction in the existence of photocatalyst employing solar energy. The properties of noble photocatalyst must be nonhazardous, economical and consume solar light properly. Heterogeneous advanced oxidation process (AOPs) is one of the best methods for wastewater treatment. In AOPs, oxidation process carried out in aqueous medium in which adsorbed water molecules oxidized into hydroxyl (-OH) radicals on the surface of catalyst. Subsequently, this procedure generally executed underneath aerobic condition. In this condition a species reduce the oxygen molecule and converted into superoxide ($O_2^{\cdot -}$) radical. Photocatalyst may be photo-chemically active in case of metal oxide-based compounds. For valence band, redox potential should be positive and for conductance band it must be effectively negative. Unluckily, there are some limitation are found to be in all AOPs process like high energy consumption, creation of iron sludge, high operational cost, etc. (Chowdhuri et al. 2015). The AOPs is a best technique for wastewater treatment, which is generally independent upon production of hydroxyl radical. The photocatalytic reaction generally prompted when a photon with energy larger than the band gap of semiconductor attacks on the surface, and the valence band to the conduction band elevation of electron occurs which generates holes in the valence band (Brunet et al. 2009). Hydroxyl radicals are highly reactive species and have tendency to degrade the organic and inorganic pollutant present in aqueous system. Over an oxidation process, hole can extract electron from water molecule and generate (OH^{\cdot}) hydroxyl radical (Lin, Liao, and Hung 2005). Hydroxyl radical and superoxide ions both are nonselective strong oxidants and have tendency to destroy the structure of all organic, inorganic and even biomolecules such as protein, lipid, and carbohydrates and can be used to purify the contaminant water molecules (Du and Gebicki 2004). The constant attack of superoxide radical and hydroxyl radical cause the photo-degradation and mineralization of organic molecules. Photocatalyst generated oxidizing agents like OH^{\cdot} , $O_2^{\cdot -}$, and H_2O_2 in the presence of sun light which are capable to destroy organic and micro-organisms. Commonly, there are some drawback to use bare photocatalyst such as agglomeration, low stability, absorbing small quantities of photon in the visible region, high recombination rate for the photo-induced electron-hole pair (Paola et al. 2012). This type of drawbacks decreases the yield and reduce the photo-efficiency of photocatalyst. Use of bare metal oxide (binary, ternary, and quaternary) nanoparticle for water treatment is very limited, due to this drawback's poor absorption of contaminants, lack of reusability, uneasy separation, highly unstable and low tendency to flocculation and nanotoxicity. As a significance of this limitations, heterogeneous photocatalyst using inorganic nanomaterials have reveal the electronic and electronic alteration using codoping, metal deposition, defect induced catalysis, and nonmetal doping (Anandan, Ohashi, and Miyachi 2010). Amongst all this approaches, selection of selected materials and photocatalyst can be as a prominent way for prevalent over this limitation of bare nanoparticles. Metal based and modified nanoparticles, bimetallic system are supported on to polymeric, carbonaceous and inorganic materials such as activated carbon, chitosan, graphene, graphene oxide, reduced graphene oxide, biochar, fullerene, carbon nanotubes enhance the stability and photocatalytic activity of metallic photocatalyst (Xu et al. 2011).

Kinetic study

The study of adsorption kinetic of MV on r-GO perform in an aqueous medium at fixed concentration (5 ppm) were distinguish the adsorption procedure (Fig S5). For r-GO, in the first 10 min adsorption increases, then reduces and extents equilibrium after 40 min. The kinematic considerations conforming to adsorption of MV at the r-GO water edge remained evaluated by pseudo first order and pseudo second-order kinetic simulations with 5 ppm of original dye concentration. Adsorption kinetics describing the MV adsorption rate is one of the important characteristics which oversight the remaining time of adsorbate adsorption on the solid-liquid boundary. Remaining chemical concentration was slow by altered time intermissions. The linear fit outcomes of the two prototypes are revealed in Figure S5. The kinetic constraints considered as of the fitting plots existed in Table S2.

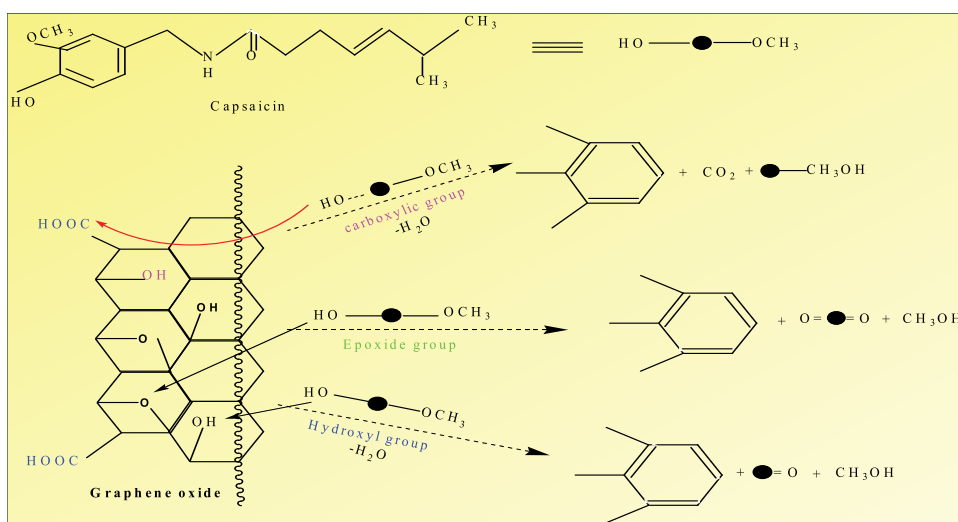
The experimental data of kinetic study was compared with other, pseudo-first-order reaction for r-GO ($R^2 = 0.97$) and for pseudo-second-order reaction ($R^2 = 1$), the correlation coefficients R^2 specified a superior fitting on pseudo-second-order calculation, which indicate the chemisorption adsorption (Figs S6 and S7).

Proposed mechanism of r-GO

CA extract contains mainly capsaicin (phenolic compounds such as capsaicinoids), All chili papers, including green chillies, contain capsaicin (8-methyl-*N*-vanillyl-6-nonenamide) which is accountable for the hot sensation associated with eating a hot pepper. Graphene oxide (GO) holds many functional groups like epoxy, hydroxyl and carboxylic clusters. Characterization studies of GO and r-GO, the mechanism of the reaction has been suggested. Established on this suggested appliance (Scheme 1) reduction of GO followed in three basic steps: initiation, propagation, and termination. In responsive hydroxyl radicals attacked the hydroxyl groups experiencing radical propagation, prominent to the construction of carbonyls. Carboxylate to decay by decarboxylation, creating CO_2 radicals. Furthestmost reduction process causes ring opening of an epoxy cluster. In last step halogenation substitution response of a hydroxyl group. The freshly designed species later this reaction that definite the reduction of GO to r-GO (Liu et al. 2011). Dye elimination competence of some earlier described r-GO produced by exhausting altered reducing agents in Table 5.

Reusability of catalyst

The properties of rejuvenated r-GO on the degradation of MV in five cycles were presented in Fig. S8. To estimate the stability of r-GO in the Fenton process, we used it frequently for several successive MV removal cycle. The solid catalyst was detached from the reaction mixture every time, wash away with ethanol, distilled water and then dried. It can be visibly seen that even though the degradation capabilities of r-GO for MV are found to be 98%-99.5% and turn over number (TON) obtained around 4. Turn over frequency (TOF) was found to be $2.6 \times 10^2 \text{ (m}^{-1}\text{)}$ for catalyst. So, r-GO displays high stability throughout MV removal since aqueous mixtures.



Scheme 1. Methodical demonstration of suggested mechanism for r-GO.

Table 5. Dye elimination competence of some beforehand described r-GO synthesized by using different reducing reagent.

Material used	Reducing agents	Dye used	Dye concentration	Percentage removal	References
Magnetite/reduced graphene oxide	Sodium acrylate and sodium acetate	Rhodamine B	5 ppm	91	Dutta, Thiyagarajan, and Bahadur (2016)
Magnetite/reduced graphene oxide	Sodium acrylate and sodium acetate	Malachite green	5 ppm	94	Upadhyay et al. (2015)
Reduced graphene oxide (RGO)/Fe ₃ O ₄ Nanocomposites	Solanum trilobatum extract	Methylene blue	93.7 μM	95.18	Xiong et al. (2011)
Chemically reduced graphene oxide	Concentrated ammonia solution (37 wt%)	Methylene blue	31.5 μM	84.8	Sun, Cao, and Lu (2011)
Copper-modified reduced graphene oxide	Sodium borohydride	Rhodamine B	5.3 μM	86	Sun et al. (2012)
Reduced graphene oxide	Capsicum annum extract	Methyl violet	5 ppm	96	This work

Conclusion

In this study, CA was used for the reduction of GO as a reducing and stabilizing agent. In this study, a modest and cost-effective method was offered for the synthesis of r-GO by the chemical reduction of exfoliated GO. The reduction method of GO was executed below aqueous medium using capsicum annum extract. It acts as a green reducing and stabilizing negotiators. This scheme avoiding the destructive and noxious gases produced throughout synthesis process. The product has been characterized over XRD, Raman spectroscopy, FTIR, FE-SEM, TGA/DTA, BET, and zeta potential provide the information for the formation of r-GO after reduction of exfoliated GO with capsicum annum. These outcomes suggest that the green and natural reducing agents can be highly effective in initiating de-oxygenation of GO. The r-GO revealed noteworthy fast adsorption competence within 60 min and the kinetic study showed a good association to a pseudo-second-order equation and the overall adsorption process MV onto r-GO.

Acknowledgments

This work was supported by the Deanship of Scientific Research (DSR), King Abdulaziz University, Jeddah, under grant no. (DF-698-130-1441). The authors, therefore, gratefully acknowledge DSR technical and financial support.

Funding

This work was supported by the Aftab Aslam Parwaz Khan-King Abdulaziz University [DF-698-130-1441].

ORCID

A. K. Singh  <http://orcid.org/0000-0001-8180-7292>

References

- Akhavan, O. G., and E. Ghaderi. 2012. Escherichia coli bacteria reduce graphene oxide to bactericidal graphene in a self-limiting manner. *Carbon* 50 (5):1853–60. doi:10.1016/j.carbon.2011.12.035.
- Alsebaei, M., A. K. Chauhan, Y. P. Arvind, M. A. Sayadi, S. A. Dalali, and H. A. Eryani. 2018. Microscopic Characterizations of Green Chilli Powder. *International Journal of Current Microbiology & Applied Sciences* 7:2488–97. doi:10.20546/ijcmas.2018.708.252.
- Anandan, S., N. Ohashi, and M. Miyachi. 2010. ZnO-based visible light photocatalyst, B&-gap engineering & multi-electron reduction by co-catalyst. *Applied Catalysis. B, Environmental* 100:502–09. doi:10.1016/j.apcatb.2010.08.029.

- Bo, Z., X. Shuai, S. Mao, H. Yang, J. Qian, and J. Chen. 2014. Green preparation of reduced graphene oxide for sensing & energy storage applications. *Scientific Reports* 4:4684. doi:10.1038/srep04684.
- Brunet, L., D. Y. Lyon, E. M. Hotze, P. J. Alvarez, and M. R. Wiesner. 2009. Comparative photoactivity & antibacterial properties of C60 fullerenes & titanium dioxide nanoparticles. *Environmental Science & Technology* 43:4355–60. doi:10.1021/es803093t.
- Chen, C. M., Q. Zhang, M. G. Yang, C. H. Huang, Y. G. Yang, and M. Z. Wang. 2012. Structural evolution during annealing of thermally reduced graphene nanosheets for application in supercapacitors. *Carbon* 50:3572–84. doi:10.1016/j.carbon.2012.03.029.
- Chowdhuri, A. R., S. Tripathy, C. Haldar, S. Chandra, B. Das, S. Roy, and S. K. Sahu. 2015. Theoretical and experimental study of folic acid conjugated silver nanoparticles through electrostatic interaction for enhance antibacterial activity. *RSC Advances* 5 (28):21515–24. doi:10.1039/C4RA16785F.
- Cui, Y., S. I. Kundalwal, and S. Kumar. 2016. Gas Barrier Performance of Graphene/polymer Nanocomposites. *Carbon* 98:313–33. doi:10.1016/j.carbon.2015.11.018.
- Davar, F., M. S. Niasari, N. Mir, K. Saberyan, M. Monemzadeh, and E. Ahmadi. 2010. Thermal decomposition route for synthesis of Mn₃O₄ nanoparticles in presence of a novel precursor. *Polyhedron* 29 (7):1747–53. doi:10.1016/j.poly.2010.02.026.
- Du, J., and J. M. Gebicki. 2004. Proteins are major initial cell targets of hydroxyl free radicals. *The International Journal of Biochemistry & Cell Biology* 36 (11):2334–43. doi:10.1016/j.biocel.2004.05.012.
- Dutta, D., S. Thiyagarajan, and D. Bahadur. 2016. SnO₂ quantum dots decorated reduced graphene oxide nanocomposites for efficient water remediation. *Chemical Engineering Journal* 297:55–65.
- Fernández, M.M.J.L., Guardia, J.I. Paredes, S. Villar-Rodil, P. Solís-Fernández, A. Martínez-Alonso and J.M.D. Tascón. 2010. Vitamin C Is an Ideal Substitute for Hydrazine in the Reduction of Graphene Oxide Suspensions. *The Journal of Physical Chemistry C* 114 (4):6426–6432. doi:doi:10.1021/jp100603h
- Gao, J., F. Liu, Y. Liu, N. Ma, Z. Wang, and X. Zhang. 2010. Environment-friendly method to produce graphene that employs vitamin C and amino acid. *Chemistry of Materials* 22 (7):2213–18. doi:10.1021/cm902635j.
- Gerster, H. 1997. The potential role of lycopene for human health. *Journal of the American College of Nutrition* 16 (2):109–26. doi:10.1080/07315724.1997.10718661.
- Gong, J. L., B. Wang, G. M. Zeng, C. P. Yang, C. G. Niu, Q. Y. Niu, and Y. Liang. 2009. Removal of cationic dyes from aqueous solution using magnetic multi-wall carbon nanotube nanocomposite as adsorbent. *Journal of Hazardous Materials* 164:1517–22. doi:10.1016/j.jhazmat.2008.09.072.
- Guo, H. L., X. F. Wang, Q. Y. Qian, F. B. Wang, and X. H. Xia. 2009. A green approach to the synthesis of graphene nanosheets. *ACS Nano* 3:2653–59. doi:10.1021/nn900227d.
- Gurbani, N., C.-P. Han, K. Marumoto, R.-S. Liu, R. J. Choudhary, and N. Chouhan. 2018. Biogenic Reduction of Graphene Oxide: An Efficient Superparamagnetic Material for Photocatalytic Hydrogen Production. *ACS Applied Energy Materials* 1 (11):5907–18. doi:10.1021/acsaem.8b00552.
- Haghighi, B., and M. A. Tabrizi. 2013. Green-synthesis of reduced graphene oxide nanosheets using rose water and a survey on their characteristics and applications. *RSC Advances* 3 (32):13365–71. doi:10.1039/c3ra40856f.
- Hashmi, A., A. K. Singh, B. Jain, and A. Singh. 2020b. Muffle atmosphere promoted fabrication of graphene oxide nanoparticle by agricultural waste. *Fullerenes, Nanotubes and Carbon Nanostructures* 28 (8):627–36. doi:10.1080/1536383X.2020.1728744.
- Hashmi, A., A. K. Singh, B. Jain, and S. A. C. Carabineiro. 2020a. Chloramine-T/N-Bromosuccinimide/FeCl₃/KIO₃ decorated Graphene oxide Nanosheets and their Antibacterial Activity. *Nanomaterials* 10:105. doi:10.3390/nano10010105.
- He, D., Z. Peng, W. Gong, Y. Luo, P. Zhao, and L. Kong. 2015. Mechanism of a green graphene oxide reduction with reusable potassium carbonate. *RSC Advances* 5 (16):11966–72. doi:10.1039/C4RA14511A.
- He, H., and C. Gao. 2010. General approach to individually dispersed, highly soluble, & conductive graphene nanosheets functionalized by nitrene chemistry. *Chemistry of Materials* 22 (17):5054–64. doi:10.1021/cm101634k.
- Jha, A. K., and K. Prasad. 2011. Green fruit of chili (*Capsicum annum* L.). *Synthesizes Nano Silver! Digest. Journal of Nanomaterials and Biotechnologies* 6:1717–23.
- Kuila, T., S. Bose, P. Khanra, A. K. Mishra, N. H. Kim, and J. H. Lee. 2012. A green approach for the reduction of graphene oxide by wild carrot root. *Carbon* 50 (3):914–21. doi:10.1016/j.carbon.2011.09.053.
- Lei, Y., Z. Tang, R. Liao, and B. Guo. 2011. Hydrolysable tannin as environmentally friendly reducer & stabilizer for graphene oxide. *Green Chemistry* 13 (7):1655–58. doi:10.1039/c1gc15081b.
- Li, Y., J. Zhu, S. Wei, J. Ryu, Q. Wang, L. Sun, and Z. Guo. 2011. Poly(propylene) nanocomposites containing various carbon nanostructures. *Macromolecular Chemistry and Physics* 212 (22):2429–38. doi:10.1002/macp.201100364.
- Lin, H. F., S. C. Liao, and S. W. Hung. 2005. The dc thermal plasma synthesis of ZnO nanoparticles for visible-light photocatalyst. *Journal of Photochemistry and Photobiology. A, Chemistry* 174:82–87. doi:10.1016/j.jphotochem.2005.02.015.
- Liu, T., L. Wang, X. Lu, J. Fan, X. Cai, B. Gao, R. Miao, J. Wang, and Y. Lv. 2017. Comparative study of the photocatalytic performance for the degradation of different dyes by ZnIn₂S₄, adsorption, active species, and pathways. *RSC Advances* 7:12292–300. doi:10.1039/C7RA00199A.

- Liu, Y., Y. Li, M. Zhong, Y. Yang, Y. Wen, and M. Wang. 2011. A green and ultrafast approach to the synthesis of scalable graphene nanosheets with Zn powder for electrochemical energy storage. *Journal of Materials Chemistry* 21 (39):15449–55. doi:10.1039/c1jm12599k.
- Mahmoodi, N. M., S. M. Maroofi, M. Mazarji, and B. G. Nabi. 2017. Preparation of modified reduced graphene oxide nanosheet with cationic surfactant and its dye adsorption ability from colored wastewater. *Journal of Surfactants and Detergents* 20 (5):1085–93. doi:10.1007/s11743-017-1985-1.
- McAllister, M. J., J. L. Li, D. H. Adamson, H. C. Schniepp, A. A. Abdala, J. Liu, and A. M. D. L. Herrera. 2017. Single sheet functionalized Graphene by oxidation and thermal expansion of graphite. *Chemistry of Materials* 19:4396–404. doi:10.1021/cm0630800.
- Minitha, C., M. Lalitha, Y. Jeyachandran, and L. Senthilkumar. 2017. Adsorption behaviour of reduced graphene oxide towards cationic and anionic dyes, Co-action of electrostatic and $\pi - \pi$ interactions. *Material Chemistry and Physics* 194:243–52. doi:10.1016/j.matchemphys.2017.03.048.
- Mohandes, F., F. Davar, and M. S. Niasari. 2010. Magnesium oxide nanocrystals via thermal decomposition of magnesium oxalate. *Journal of Physics and Chemistry of Solids* 71 (12):1623–28. doi:10.1016/j.jpccs.2010.08.014.
- Motahari, F., M. R. Mozdianfar, F. Soofiv, and M. S. Niasari. 2013. NiO Nanostructures, Synthesis, Characterization and Photocatalyst Application in Dye Pollution Wastewater Treatment. *RSC Advances* 4:27654–60. doi:10.1039/c4ra02697g.
- Namiki, M. 1990. Antioxidants/antimutagens in food. *CRC Critical Review in Food Science and Nutrition* 29:273–300.
- Niasari, M. S., D. Ghanbari, and M. R. L. Estarki. 2012. Star-shaped PbS nanocrystals prepared by hydrothermal process in the presence of thioglycolic acid. *Polyhedron* 35 (1):149–53. doi:10.1016/j.poly.2012.01.010.
- Niasari, M. S., M. R. L. Estarki, and F. Davar. 2008. Controllable synthesis of nanocrystalline CdS with different morphologies by hydrothermal process in the presence of thioglycolic acid. *Chemical Engineering Journal* 145 (2):346–50. doi:10.1016/j.cej.2008.08.040.
- Niyogi, S., E. Bekyarova, M. E. Itkis, J. L. McWilliams, M. A. Hamon, and R. C. Haddon. 2006. Solution properties of graphite & graphene. *Journal of the American Chemical Society* 128 (24):7720–21. doi:10.1021/ja060680r.
- Noha, A., A. Alseroury, R. Kumar, T. Almeelbi, and M. A. Barakat. 2019. Synthesis of Graphene Oxide/Silica/Carbon Nanotubes Composite for Removal of Dyes from Wastewater. *Earth Systems and Environment* 3: 651–659. doi:10.1007/s41748-019-00109-w
- Palozza, P., and N. Krinsky. 1992. Antioxidant effects of carotenoids in vivo and in vitro, an overview. *Methods in Enzymology* 213:403–20.
- Paola, A. D., L. E. Garcia, G. Marci, and L. Palmisano. 2012. A survey of photocatalytic materials for environmental remediation. *Journal of Hazardous Materials* 211-212:3–29. doi:10.1016/j.jhazmat.2011.11.050.
- Pavoski, G., T. Maraschin, F. D. C. Fim, N. M. Balzaretto, G. B. Galland, C. S. Moura, and N. R. D. S. Basso. 2017. Few layer reduced graphene oxide, evaluation of the best experimental conditions for easy production. *Material Research* 20:53–61. doi:10.1590/1980-5373-mr-2015-0528.
- Pendolino, F., and N. Armata. 2017. *Graphene oxide in environmental remediation process*. Springer. 5–21. ISBN978-3-319-60428-2.
- Peng, H., L. Meng, L. Niu, and Q. Lu. 2012. Simultaneous reduction & surface functionalization of graphene oxide by natural cellulose with the assistance of the ionic liquid. *Journal of Physical Chemistry C* 116 (30):16294–99. doi:10.1021/jp3043889.
- Pimenta, M. A., G. Dresselhaus, M. S. Dresselhaus, L. G. Cancado, A. Jorio, and R. Saito. 2007. Studying disorder in graphite-based systems by Raman spectroscopy. *Physical Chemistry Chemical Physics* 9:1276–90. doi:10.1039/B613962K.
- Ray, A. K., R. K. Sahu, V. Rajinikanth, H. Bapari, M. Ghosh, and P. Paul. 2012. Preparation and characterization of graphene and Ni-decorated graphene using flower petals as the precursor material. *Carbon* 50 (11):4123–29. doi:10.1016/j.carbon.2012.04.060.
- Seo, M., D. Yoon, K. S. Hwang, J. W. Kang, and J. Kim. 2013. Supercritical alcohols as solvents and reducing agents for the synthesis of reduced graphene oxide. *Carbon* 64:207–18. doi:10.1016/j.carbon.2013.07.053.
- Shulga, Y. M., S. A. Baskakov, E. I. Knerelman, G. I. Davidova, E. R. Badamshina, N. Y. Shulga, ... V. M. Martynenko. 2014. Carbon nanomaterial produced by microwave exfoliation of graphite oxide, New insights. *RSC Advances* 4:587–92. doi:10.1039/C3RA43612H.
- Sun, H., L. Cao, and L. Lu. 2011. Magnetite/reduced graphene oxide nanocomposites, One step solvothermal synthesis and use as a novel platform for removal of dye pollutants. *Nano Research* 4:550–62. doi:10.1007/s12274-011-0111-3.
- Sun, H., S. Liu, G. Zhou, H. M. Ang, M. O. Tade, and S. Wang. 2012. Reduced graphene oxide for catalytic oxidation of aqueous organic pollutants. *ACS Applied Materials & Interfaces* 4:5466–71. doi:10.1021/am301372d.
- Thakur, S., and N. Karak. 2012. Green reduction of graphene oxide by aqueous phytoextracts. *Carbon* 50 (14):5331–39. doi:10.1016/j.carbon.2012.07.023.
- Toh, S. Y., K. S. Loh, S. K. Kamarudin, and W. R. W. Daud. 2014. Graphene production via electrochemical reduction of graphene oxide: Synthesis and characterisation. *Chemical Engineering Journal* 251:422–34. doi:10.1016/j.cej.2014.04.004.

- Upadhyay, R. K., N. Soin, G. Bhattacharya, S. Saha, A. Barman, and S. S. Roy. 2015. Grape extract assisted green synthesis of reduced graphene oxide for water treatment application. *Materials Letters* 160:355–58. doi:10.1016/j.matlet.2015.07.144.
- Wang, Y., Z. Shi, and J. Yin. 2011. Facile synthesis of soluble graphene via a green reduction of graphene oxide in tea solution and its biocomposites. *ACS Applied Materials & Interfaces* 3 (4):1127–33. doi:10.1021/am1012613.
- Xiao, M., L. Sun, J. Liu, Y. Li, and K. Gong. 2002. Synthesis and properties of polystyrene/graphite nanocomposites. *Polymer* 43 (8):2245–48. doi:10.1016/S0032-3861(02)00022-8.
- Xie, G., M. Forslund, and J. Pan. 2014. Direct electrochemical synthesis of reduced graphene oxide (rGO)/copper composite films and their electrical/electroactive properties. *ACS Applied Materials & Interfaces* 6 (10):7444–55. doi:10.1021/am500768g.
- Xiong, Z., Zhang L.L., and Zhao, X.S. 2011. Visible-Light-Induced Dye Degradation over Copper-Modified Reduced Graphene Oxide, *Chemistry European Journal* 17 (8): 2428–2434. doi. 10.1002/chem.201002906
- Xu, T., L. Zhang, H. Cheng, and Y. Zhu. 2011. Significantly enhanced photocatalytic performance of ZnO via graphene hybridization and the mechanism study. *Applied Catalysis B: Environmental* 101 (3–4):382–87. doi:10.1016/j.apcatb.2010.10.007.
- Yusuf, M., F. Elfgi, S. A. Zaidi, E. Abdullah, and M. A. Khan. 2015. Applications of graphene and its derivatives as an adsorbent for heavy metal and dye removal: A systematic and comprehensive overview. *RSC Advances* 5 (62):039250420. doi:10.1039/C5RA07223A.
- Zhang, M., Q. Yao, C. Lu, Z. Li, and W. Wang. 2014. Layered double hydroxide–carbon dot composite: High-performance adsorbent for removal of anionic organic dye. *ACS Applied Materials & Interfaces* 6 (22):20225–33. doi:10.1021/am505765e.
- Zhu, H., Y. Fu, R. Jiang, J. Yao, L. Liu, Y. Chen, L. Xiao, and G. Zeng. 2013. Preparation, characterization and adsorption properties of chitosan modified magnetic graphitized multi-walled carbon nanotubes for highly effective removal of a carcinogenic dye from aqueous solution. *Applied Surface Science* 285:865–73. doi:10.1016/j.apsusc.2013.09.003.
- Zhu, Y., S. Murali, W. Cai, X. Li, J. W. Suk, J. R. Potts, and R. S. Ruoff. 2010. Graphene and graphene oxide: Synthesis, properties, and applications. *Advanced Materials* 22 (35):3906–24. doi:10.1002/adma.201001068.